ARTICLE NO. 78-207R

J80-032

Computations of Jet Impingement on a Flat Surface

20007

A. Rubel*
Grumman Aerospace Corporation, Bethpage, N.Y.

An incompressible, inviscid rotational flow model is used to represent the normal impingement of axisymmetric jets and the oblique impingement of two-dimensional jets upon a flat surface. The Poisson-type equation that results from this formulation is cast into suitable finite-difference form and solved by relaxation techniques. Results, in terms of the ground plane pressure distribution, centerline velocity decay, and oblique impingement flowfield structure, compare well with observations.

Introduction

THE behavior of turbulent jet impingement flowfields is of considerable importance to the performance of VTOL aircraft in ground effect. In this connection, theoretical analyses of such flows have been concerned with solving either the full Navier-Stokes equations[1-4] or finding separate solutions for several component regions (for example, mixing zone, impingement zone, wall jet) that are then coupled to provide an overall solution.[5-7] The advantage of the latter approach is that each region may be represented by models closely related to the physics of the problem and relatively accurate engineering solutions obtained with comparatively simple methods. Within the context of this approach, scaling analyses[8,9] indicate that the details of the impingement region are dominated by a balance of the pressure forces due to flow deflection and the inertial forces of convection.

In this study, a variety of incompressible impingement problems are considered, under the assumption that the flow within the impingement zone can be treated as an inviscid, rotational flow. Axisymmetric jets impinging normally and two-dimensional jets impinging obliquely form a set of problems that can be formulated in two dimensions with vorticity/radius or vorticity, respectively, conserved along streamlines. Both developing and fully developed jet velocity profiles are considered as entrance conditions to the impingement region and finite-difference techniques are used to solve the governing equations. The results are compared with observations in order to determine the range of validity of the inviscid rotational model with respect to the prediction of the ground plane pressure distribution and the structure of the oblique impingement flowfield.

Formulation

The normal impingement of axisymmetric jets and the normal/oblique impingement of two-dimensional jets are represented here by the equations governing inviscid rotational flow. The jets are considered to be far from the impingement plane, so that influx conditions are not affected by the jet deflection. The formulation is given in terms of dimensionless quantities; velocities are scaled by the maximum jet velocity, distance by the jet half-width (i.e., distance measured along the perpendicular from the jet centerline to the point at which the velocity is half the maximum), and pressures by the total pressure at the jet centerline. Ambient and jet static pressure are taken to be zero without loss of generality.

A coordinate system is chosen with z directed perpendicular to the ground plane, positive outward, and x directed along the ground plane, such that the origin is at the intersection of the ground plane and the jet centerline (Fig. 1). Eliminating pressure from the x and z momentum equations yields the vorticity equation

$$\frac{d(\omega/x^n)}{dt} = u\frac{\partial(\omega/x^n)}{\partial x} + w\frac{\partial(\omega/x^n)}{\partial z} = 0 \tag{1}$$

where u and w are the velocities in the x and z directions, respectively, n is an index of the flow character (axisymmetric $n=1$, two-dimensional $n=0$), and ω is the vorticity defined by

$$\omega = \frac{\partial u}{\partial z} - \frac{\partial w}{\partial x} \tag{2}$$

A dimensionless stream function

$$\frac{\partial \psi}{\partial x} = -x^n w, \quad \frac{\partial \psi}{\partial z} = x^n u \tag{3}$$

assures satisfaction of mass conservation and, when combined with the definition of vorticity, produces the Poisson-type equation that provides the basis for the ensuing analysis

$$\frac{\partial^2 \psi}{\partial z^2} + x^n \frac{\partial}{\partial x}\left(\frac{1}{x} n \frac{\partial \psi}{\partial x}\right) - x^{2n}\left(\frac{\omega}{x^n}\right) = 0 \tag{4}$$

The unifying feature of the flows considered here is that the vorticity function, ω/x^n, is conserved along stream surfaces and, in the absence of separation bubbles, is fully specified in terms of the incoming jet stream function. The pressure is determined from an auxiliary Bernoulli equation

$$p + u^2 + w^2 = f(\psi) \tag{5}$$

which follows from the vector momentum equation. This relationship implies that the total pressure is conserved on stream surfaces and completes the formulation of the problem.

Although a unified treatment of the class of flows to be investigated has been presented to this point, it is advantageous to further categorize the flows to more clearly indicate the manner in which boundary conditions are prescribed and special cases are developed. For normal impingement, there is flow symmetry about the jet centerline

Presented as Paper 78-207 at the AIAA 16th Aerospace Sciences Meeting, Huntsville, Ala., Jan. 16-18, 1978; submitted March 14, 1979; revision received July 31, 1979.

Index categories: Jets, Wakes, and Viscid-Inviscid Flow Interactions.

*Staff Scientist, Research Department. Member AIAA.

($x=0$) and only the domain $x\geq 0$ need be considered. The boundary conditions are:

$$\psi(0,z)=0 \qquad \text{symmetry} \tag{6a}$$

$$\frac{\partial\psi}{\partial x}(\infty,z)=0 \qquad \text{parallel outflow} \tag{6b}$$

$$\psi(x,0)=0 \qquad \text{ground plane} \tag{6c}$$

$$\psi(x,\infty)=\psi(x) \qquad \text{jet inflow} \tag{6d}$$

The boundary condition at $x\to\infty$ can be replaced by a stream function distribution $\psi(z)$ (e.g., Ref. 10) and it is intructive to demonstrate the relationship between this distribution and condition (6d), as well as the implications of condition (6b).

Consider the points (X,z) for $X\to\infty$ and (x,Z) for $Z\to\infty$ in order to determine a relationship between x and z such that these points lie on the same streamline. The boundary conditions (6b, d) imply that when $X\to\infty$ $(Z\to\infty)$, the second (first) term of Eq. (4) becomes negligible and x and z are related parametrically through $\omega/x^n(\psi)$. For the axisymmetric case then

$$\left(\frac{1}{X^2}\frac{\partial^2\psi}{\partial z^2}\right)_X=\left[\frac{1}{x}\frac{\partial}{\partial x}\left(\frac{1}{x}\frac{\partial\psi}{\partial x}\right)\right]_Z$$

so that

$$\frac{1}{X^2}\left[\frac{\partial^2\psi}{\partial x^2}\left(\frac{\partial x}{\partial z}\right)^2+\frac{\partial\psi}{\partial x}\frac{\partial^2 x}{\partial z^2}\right]=\frac{1}{x^2}\frac{\partial^2\psi}{\partial x^2}-\frac{1}{x^3}\frac{\partial\psi}{\partial x}$$

and, equating coefficients of the stream function derivatives,

$$X\frac{\partial^2 x}{\partial z^2}=\frac{\partial}{\partial z}\left(x\frac{\partial x}{\partial z}\right)-\left(\frac{\partial x}{\partial z}\right)^2=-\frac{X^2}{x^2},\quad \frac{\partial x}{\partial z}=\frac{X}{x}$$

which has as its solution $x^2=2Xz$. Thus, for the axisymmetric case,

$$\psi(X,z)=\psi(\sqrt{2Xz},\ Z) \tag{7a}$$

and, in a similar fashion, it can be shown that for two-dimensional normal impingement,

$$\psi(X,z)=\psi(z,Z) \tag{7b}$$

The boundary condition (6b) can be recovered by noting that

$$\left(\frac{\partial\psi}{\partial x}\right)_X=\left(\frac{\partial\psi}{\partial x}\right)_Z\left(\frac{\partial x}{\partial X}\right)_Z$$

and, thus,

$$\left(\frac{\partial\psi}{\partial x}\right)_X=0$$

for the two-dimensional case and

$$\left(\frac{\partial\psi}{\partial x}\right)_X=-zw(\sqrt{2Xz},\ Z)$$

for the axisymmetric case. For the velocity profile considered here (Table 1), it can be seen that

$$\left(\frac{\partial\psi}{\partial x}\right)_{X\to\infty}=\frac{z}{(1+2c_2Xz)^2}\leq\frac{1}{8c_2X}$$

so that the parallel flow boundary condition is compatible with the specification of the far-field velocity profile.

Several jet profiles are chosen (Fig. 2) in order to evaluate the effect of fully developed vis-a-vis developing flow on the ground plane pressure distribution. The functional form of these profiles[11] and the derived stream function distributions and vorticity functions are given in Table 1. The vorticity forcing function is implicitly related to the stream function in the two-dimensional developing jet cases; hence, recasting Eq. (4) in a new dependent variable $\xi(\psi)$, defined in Table 1, is desirable. For these cases, the governing equation becomes

$$\frac{\partial^2\xi}{\partial x^2}+\frac{\partial^2\xi}{\partial z^2}+\frac{2}{\sqrt{\pi}}\frac{e^{-\xi^2}}{(1+\mathrm{erf}\xi)}\left[\left(\frac{\partial\xi}{\partial x}\right)^2+\left(\frac{\partial\xi}{\partial z}\right)^2-\frac{1}{\sigma^2}\right]=0 \tag{8}$$

where σ is a spreading parameter for the profiles and the boundary conditions are

$$\xi(0,z)=1/\sigma \tag{9a}$$

$$\frac{\partial\xi}{\partial x}(\infty,z)=0 \tag{9b}$$

$$\xi(x,0)=1/\sigma \tag{9c}$$

$$\xi(x,\infty)=(1-x)/\sigma \tag{9d}$$

Equation (4) remains valid for the oblique two-dimensional impingement cases (only fully developed profiles are considered), but the independent variables are transformed so that the new $\bar{z}$ coordinate is aligned with the jet centerline. The new $\bar{x}$ coordinate is measured from the jet centerline in a direction parallel to the ground plane. Therefore,

$$\bar{z}=z/\sin\beta,\quad \bar{x}=x-z/\tan\beta \tag{10}$$

and Eq. (4) becomes

$$\frac{\partial^2\psi}{\partial\bar{x}^2}+\frac{\partial^2\psi}{\partial\bar{z}^2}-2\cos\beta\frac{\partial^2\psi}{\partial\bar{x}\partial\bar{z}}+2c_1^2\sin^2\beta\psi(1-c_1^2\psi^2)=0 \tag{11}$$

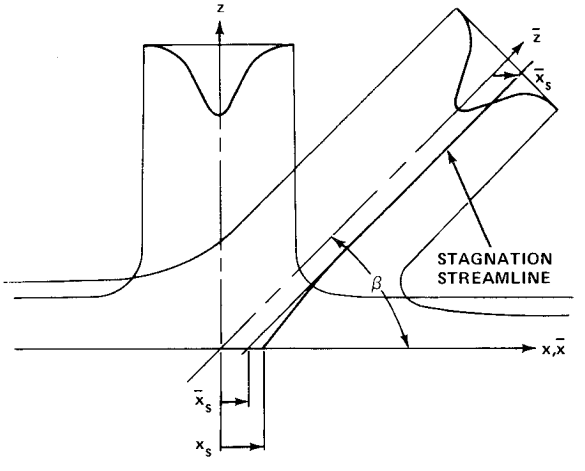

Fig. 1 Schematic of the jet impingement problem.

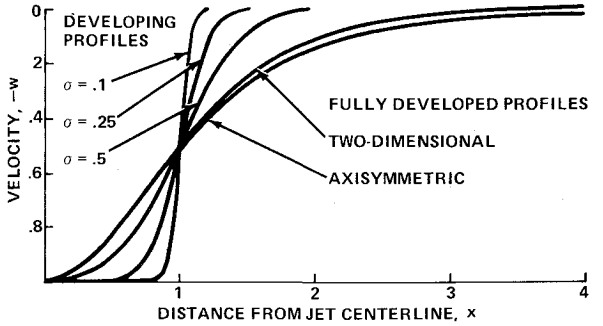

Fig. 2 Jet velocity profiles.

Table 1 Rotational jet flow parameters

	Velocity, $-w(x)$	Stream function, $\psi(x)$	Velocity function, $-\omega/x^{n(\psi)}$
Axisymmetric fully developed	$(1+c_2x^2)^{-2}$ $c_2=\sqrt{2}-1$	$x^2/2(1+c_2x^2)$	$4c_2(1-2c_2\psi)^3$
Two-dimensional fully developed	$(1-\tanh^2 c_1x)$ $c_1=\tanh^{-1}(1/\sqrt{2})$	$\frac{1}{c_1}\tanh(c_1x)$	$2c_1^2\psi(1-c_1^2\psi^2)$
Two-dimensional developing	$\frac{1}{2}\{1+\mathrm{erf}[(1-x)/\sigma]\}$ $\sigma=0.1, 0.25, 0.5$	$\frac{\sigma}{2}\int_{1/\sigma}^{(1-x)/\sigma}(1+\mathrm{erf}\xi)\,d\xi$ $\xi=(1-x)/\sigma$	$\frac{e^{-\xi^2(\psi)}}{\sigma\sqrt{\pi}}$

where β is the angle between the jet centerline and the ground plane (Fig. 1). The stream function is still related to the velocities u and w by Eq. (3) and, for $\beta=90$ deg, Eq. (11) reduces to Eq. (4) with $\bar{x}=x$, $\bar{z}=z$. The boundary conditions for the oblique impingement problem are:

$$\frac{\partial\psi}{\partial\bar{x}}(\pm\infty,\bar{z})=0 \qquad (12a,b)$$

$$\psi(\bar{x},\infty)=1/c_1\ \tanh(c_1\bar{x}\sin\beta) \qquad (12c)$$

$$\psi(\bar{x},0)=\psi_s \qquad (12d)$$

where ψ_s is the value of the stagnation stream function. It is easily demonstrated that, for the oblique impingement case,

$$\psi(\bar{X},\bar{z})=\psi(\bar{x}_s+\bar{z},\ \bar{Z})\ \bar{X}\to\infty,\ \ \bar{Z}\to\infty \qquad (13)$$

where $\bar{x}_s$ is the distance in the $\bar{x}$ coordinate from the jet centerline to the stagnation streamline at the jet exit. Using this description of the ground plane flow far from the origin, a balance of momentum in the x direction yields the value for ψ_s. Thus,

$$2\cos\beta\int_0^{\psi_\infty}\bar{w}\,d\psi=\int_{\psi_s}^{\psi_\infty}\bar{u}\,d\psi+\int_{\psi_s}^{\psi_{-\infty}}\bar{u}\,d\psi$$

where $\bar{w}$ and $\bar{u}$ are the velocities in the jet centerline (influx) and ground plane (efflux) directions, respectively. Utilizing the fully developed profile information, i.e.,

$$-\bar{w}=\bar{u}=1-c_1^2\psi^2,\quad \psi_{\pm\infty}=\pm 1/c_1$$

produces the desired result

$$\cos\beta=3/2\quad c_1\psi_s(1-c_1^2\psi_s^2/3) \qquad (14)$$

and completes the formulation for the impingement problems considered here.

Method of Solution

Finite-difference techniques[10] are used to solve the governing Poisson-type equation for the stream function field. Since the decaying influx and efflux velocity profiles far from the origin are infinite in extent, the calculation of a bounding jet streamline is not of concern. Instead, the extent of the physical domain chosen for the application of the boundary conditions must be large enough that the results in the ground plane are converged (i.e., a larger domain produces no change in results). The normal impingement problem is solved in the rectangular region of height Z and width X (Fig. 3a). Furthermore, to match the stream function at the corner point (X,Z) requires that $X=2Z$ for the axisymmetric case [Eq. (7a)] and $X=Z$ for the two-dimensional case [Eq. (7b)]. (Numerical experiments indicate that such a domain produces improved mesh convergence properties.) The oblique impingement problem is solved in the numerically rectangular region of height, $\bar{Z}$, and width, $2\bar{X}$ (Fig. 3b). The displacement of the stagnation streamline, $\bar{x}_s$, is small enough in the problems considered here that, at the corner points $(\pm\bar{X},\bar{Z})$, the stream function is nearly matched [Eq. (13)].

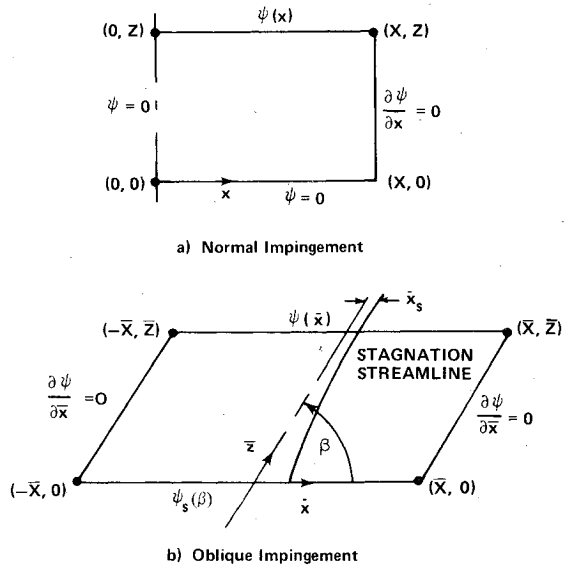

Fig. 3 Physical domain and boundary conditions for finite-difference analysis.

The numerical representation of Eqs. (4) and (8) makes use of a uniform mesh with spacing defined by

$$\Delta x=X/(N_X-1)\qquad \Delta z=Z/(N_Z-1)$$

where N_X and N_Z are the number of points in the x and z directions, respectively. Using central differencing for the derivatives of the dependent variable results in the internal point (i,j) finite-difference equations for the axisymmetric case [i.e., Eq. (4), $n=1$],

$$-\psi_{i+1,j}+[2+D^2(x_{-j/2}+x_{j/2})$$

$$-8c_2^2x_{i,j}^2(1-2c_2\psi_{i,j})^2]\psi_{i,j}^*$$

$$-\psi_{i-1,j}^*=D^2(x_{j/2}\psi_{i,j+1}+x_{-j/2}\psi_{i,j-1})$$

$$+4c_2x_{i,j}^2(1-2c_2\psi_{i,j}^2)(\Delta z)^2 \qquad (15)$$

Table 2 Numerical parameters for selected impingement computations

	Axisymmetric normal	Two-dimensional									
		Normal				Oblique (fully developed)					
	Fully developed	Fully developed	σ 0.5	0.25	0.1	β, deg 80	70	60	50	40	30
$X(2\bar{X})$[a]	8	5	5	5	5	10	10	12	12	16	20
$Z(\bar{Z})$	4	5	5	5	5	5	5	6	6	8	10
$N_X(N_{2\bar{X}})$	81	41	41	41	41	41	41	81	41	41	41
$N_Z(N_{\bar{Z}})$	161	41	41	41	41	21	21	41	21	21	21
ϵ	10^{-6}	10^{-6}	10^{-5}	10^{-5}	10^{-5}	10^{-6}	10^{-6}	10^{-6}	10^{-6}	10^{-6}	10^{-6}
ν	438	370	338	428	1938	741	816	3401	1063	1435	1799

[a]Quantities in parentheses refer to the oblique impingement cases. X = width, Z = height, N = number of points, ϵ = tolerance, ν = number of iterations.

where $D=\Delta z/\Delta x$ and $x_{\pm j/2}=x_{i,j}/(x_{i,j}\pm\Delta x/2)$, for the two-dimensional, fully developed case (i.e., Eq. (4), $n=0$),

$$-\psi^*_{i+1,j}+[2(1+D^2)-2c_1^2(1-c_1^2\psi_{i,j}^2)(\Delta z)^2]\psi^*_{i,j}$$
$$-\psi^*_{i-1,j}=D^2(\psi_{i,j+1}+\psi_{i,j-1}) \tag{16}$$

and for the two-dimensional developing flow case [i.e., Eq. (8)]

$$-(1+A_{i,j})\xi^*_{i+1,j}+2(1+D^2)\xi^*_{i,j}-(1-A_{i,j})\xi^*_{i-1,j}$$
$$=D^2(\xi_{i,j+1}+\xi_{i,j-1})+B_{i,j}\left[\frac{D^2}{4}(\xi_{i,j+1}-\xi_{i,j-1})^2-(\Delta z/\sigma)^2\right] \tag{17}$$

where

$$A_{i,j}=\frac{B_{i,j}}{4}(\xi_{i+1,j}-\xi_{i-1,j})$$

$$B_{i,j}=\frac{2}{\sqrt{\pi}}\frac{e^{-\xi_{i,j}^2}}{(1+\mathrm{erf}\,\xi_{i,j})}$$

These equations are modified slightly at $x=X$ by the use of additional fictitious points to satisfy the gradient boundary condition by reflection. Equations (15-17) are arranged for line relaxation by tridiagonal solution techniques. The asterisk superscript refers to an intermediate value of the dependent variable; coefficients of these variables and the right sides of the equations refer to previous values of these quantities (i.e., νth iterative values). The $(\nu+1)$ values are obtained by the relaxation formula:

$$\psi_{i,j}^{\nu+1}=(1-r)\psi_{i,j}^{\nu}+r\psi^*_{i,j}$$

where $0<r<1$ indicates underrelaxation and $1<r<2$ indicates overrelaxation. The nonlinear vorticity forcing functions have been arranged in Eqs. (15-17) so that they are partially included in the implicit line relaxation calculation.

A similar representation of Eq. (11), for oblique impingement, makes use of a uniform mesh with spacings

$$\Delta\bar{x}=\frac{2\bar{X}}{N_{2\bar{X}}-1}\qquad\Delta\bar{z}=\frac{\bar{Z}}{N_{\bar{Z}}-1}$$

where $N_{2\bar{X}}$ and $N_{\bar{Z}}$ are the number of points in the $\bar{X}$ and $\bar{Z}$ directions, respectively, and yields the internal point finite-difference equation

$$-\psi^*_{i+1,j}+2[1+\bar{D}^2-c_1^2(1-c_1^2\psi_{i,j}^2)\sin^2\beta(\Delta z)^2]\psi^*_{i,j}-\psi^*_{i-1,j}$$
$$=\bar{D}^2(\psi_{i,j+1}+\psi_{i,j-1})-\frac{\bar{D}}{2}\cos\beta(\psi_{i+1,j+1}+\psi_{i-1,j-1}$$
$$-\psi_{i+1,j-1}-\psi_{i-1,j+1}) \tag{18}$$

where $\bar{D}=\Delta\bar{z}/\Delta\bar{x}$.

The ground plane velocity is a derived quantity of considerable importance, since it determines the ground plane pressure by Bernoulli's equation. From Eq. (3), and the appropriate transformations, this velocity is given, to second order in mesh height, by

$$u(x,0)=[\psi(x,\Delta z)-\tfrac{1}{2}(\partial^2\psi/\partial z^2)(x,0)(\Delta z)^2]/x^n\Delta z \tag{19a}$$

for fully developed normal impingement, by

$$u(x,0)=\tfrac{1}{2}(1+\mathrm{erf}(1/\sigma))[1-\sigma\xi(x,\Delta z)]/\Delta z \tag{19b}$$

for the normal impingement developing flow and by

$$u(\bar{x},0)=-[\psi(\bar{x},\Delta\bar{z})-\psi_s-\tfrac{1}{2}(\partial^2\psi/\partial\bar{z}^2)(\bar{x},0)(\Delta\bar{z})^2]/\Delta\bar{z}\sin\beta \tag{19c}$$

for two-dimensional oblique impingement. The value of the second derivative of the stream function can be found from the governing differential equations evaluated at the ground plane. For the fully developed normal impingement cases, this is easily done: $(\partial^2\psi/\partial z^2=0$ in two-dimensional flow, $\partial^2\psi/\partial z^2=x\omega$ in axisymmetric flow). The oblique impingement case, however, requires calculation of a row of coupled fictitious points located at $\bar{z}=-\Delta\bar{z}$ [via Eq. (18)] in order to represent the stream function second derivative; that is,

$$(\partial^2\psi/\partial\bar{z}^2)(\bar{x},0)=[\psi(\bar{x},\Delta\bar{z})-2\psi_s+\psi(x,-\Delta\bar{z})]/(\Delta\bar{z})^2$$

The ground plane pressure is evaluated from

$$p(\bar{x},0)=\bar{w}^2(\bar{x}_s,\bar{Z})-\bar{u}^2(\bar{x},0) \tag{20}$$

A considerable number of calculations are necessary (e.g., Table 2) in order to determine the character of the numerical solution. Initial estimates for all computations reported herein are obtained by linear interpolation between the ground and jet exit stream function conditions. The successive relaxation procedure is applied until a convergence given by

$$\psi_{i,j}^{\nu+1}-\psi_{i,j}^{\nu}\le\epsilon|\psi_{i,j}^{\nu}|_{\max} \tag{21}$$

is obtained. It is found that the convergence parameter $\epsilon=10^{-5}$ is sufficient so that when ϵ is reduced by an order of magnitude, the maximum velocity variation at a ground plane point is less than 10^{-3}.

The domains of integration and mesh widths indicated in Table 2 for fully developed normal impingement reproduce the parallel flow conditions at $x=X$ (i.e., Eqs. (7a) and (7b) are satisfied). It can be shown that the criterion $(X\Delta z)^2\ll 1$ must be satisfied in addition to condition (7a) in order for the axisymmetric ground plane velocity to achieve its asymptotic value, $u(X,0)\to 1$. The case tabulated, for example, has a slight overshoot in velocity beginning at $x=3.7$ and reaching a maximum of 1.6% at $x\simeq X=8$.

Table 3 Comparison of computed and exact ground plane force and moment as a function of impingement angle

β, deg	F (calc)	F (exact)	M_0 (calc)	M_0 (exact)
80	1.535	1.490	−0.1972	−0.2005
70	1.456	1.422	−0.3958	−0.4059
60	1.321	1.310	−0.6120	−0.6219
50	1.170	1.159	−0.8360	−0.8563
40	0.977	0.972	−1.140	−1.121
30	0.750	0.756	−1.462	−1.436

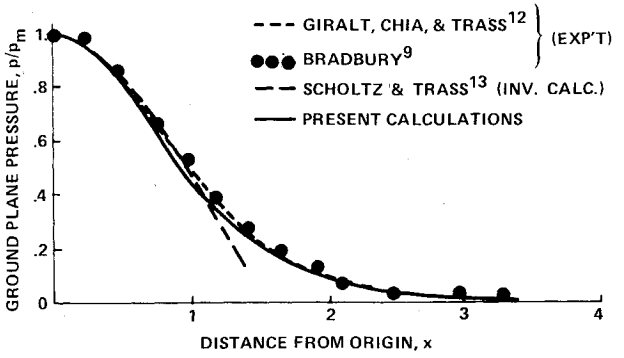

Fig. 4 Ground plane pressure distribution, axisymmetric normal impingement.

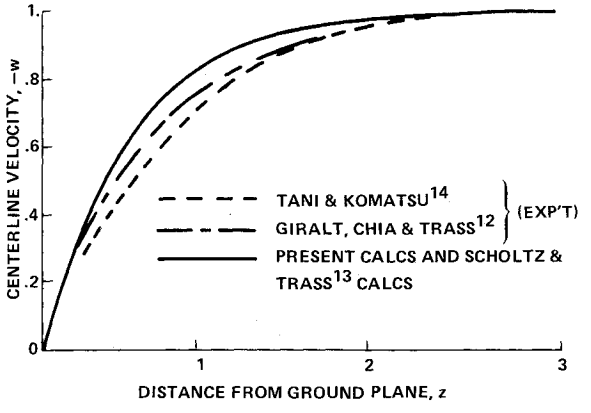

Fig. 5 Centerline velocity decay, axisymmetric normal impingement.

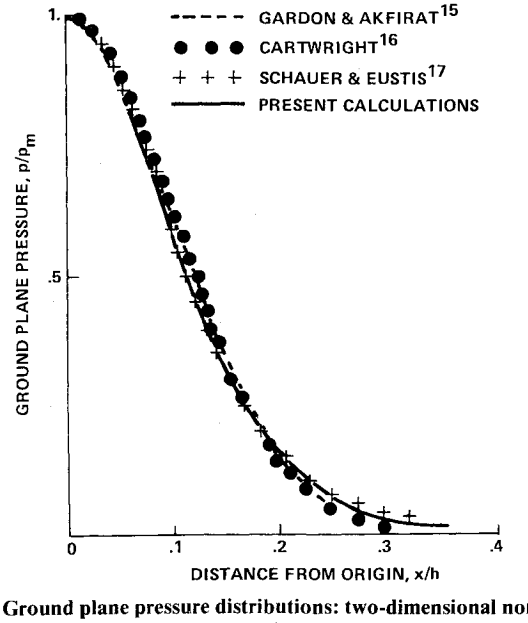

Fig. 6 Ground plane pressure distributions: two-dimensional normal impingement, fully developed jet profile.

As might be expected from a glance at Fig. 2, the developing flow cases are the most difficult to compute. The resolution of the jet velocity profiles with a uniform mesh becomes impractical for spreading parameters, $\sigma \lesssim 0.1$. Furthermore, the nature of the variable ξ is such that it grows negatively without bound as the width of the numerical domain is increased. A cutoff, such that $\xi \geq -3.49$, is used to restrict this growth and only points satisfying this criterion are considered within the domain governed by Eq. (17). This procedure, along with appreciable underrelaxation (e.g., $r = 0.3$ for $\sigma = 0.1$), provides converged solutions which recover the asymptotic ground plane velocity, even for the smallest spreading parameter (i.e., $u(X,0,) = 0.98$ at $\sigma = 0.1$).

Convergence in the oblique impingement case requires a domain that increases as the inclination angle, β, departs from 90 deg. Numerical experiments indicate that $\bar{Z} \simeq 5/\sin\beta$ and $\bar{X} = \bar{Z}$ [from Eq. (13)] provides an adequate domain for these computations. The mesh width convergence at $\beta = 60$ deg is such that a 41×21 grid produces ground plane velocities

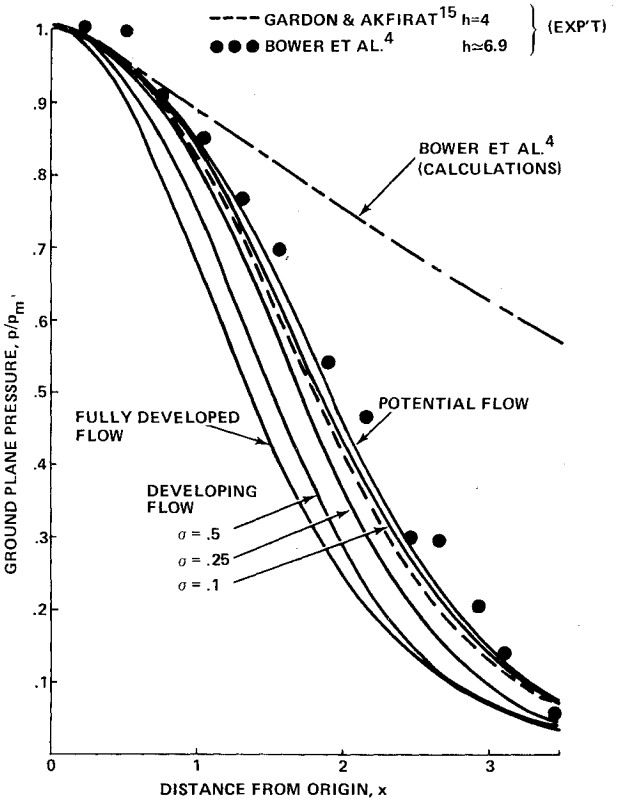

Fig. 7 Ground plane pressure distributions: two-dimensional normal impingement, fully developed, and developing jet profiles.

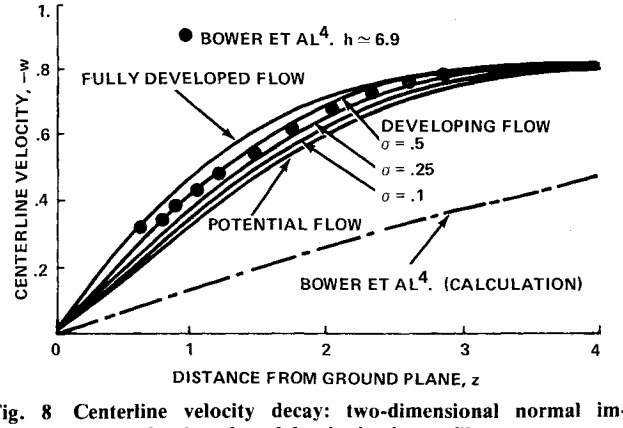

Fig. 8 Centerline velocity decay: two-dimensional normal impingement, fully developed, and developing jet profiles.

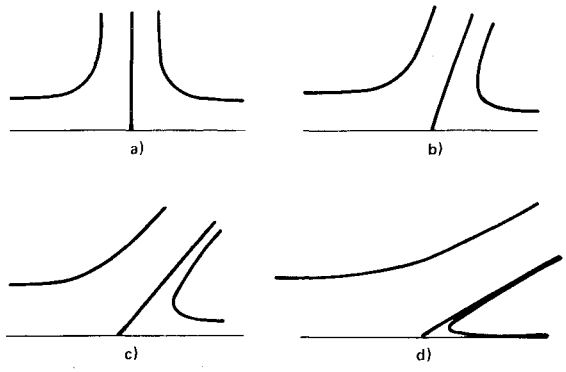

Fig. 9 Computations of jet half-width and stagnation streamlines: a) $\beta = 90$ deg, b) $\beta = 70$ deg, c) $\beta = 50$ deg, d) $\beta = 30$ deg.

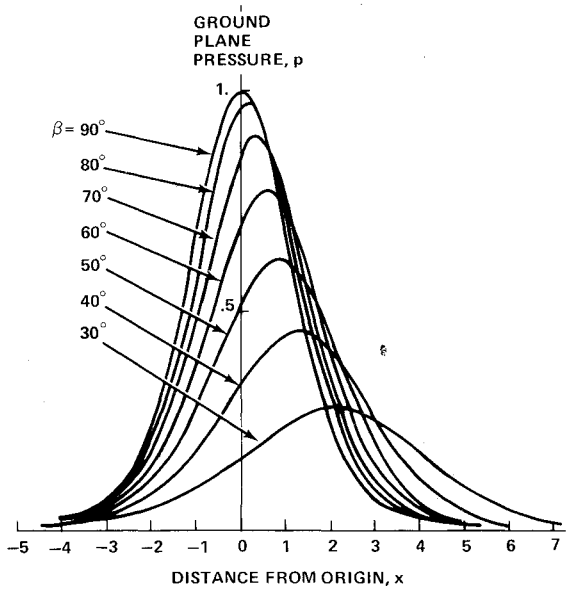

Fig. 10 Fully developed flow ground plane pressure distribution computations for two-dimensional oblique jet impingement.

within 1% of those predicted by an 81×41 grid. A similar result is found for the normal impingement case. In order to further estimate the convergence properties of the oblique impingement cases of Table 2, the resultant force on the ground plane and the moment about the origin are computed from the numerical distribution of the ground plane pressure and compared with their exact values, assuming recovery of the initial profiles at large $\bar{X}$ (i.e., Eq. (13) is satisfied). Thus,

$$F(\text{calc}) = \tfrac{1}{2}\int_{-\bar{X}}^{\bar{X}} p\,d\bar{x}$$

$$F(\text{exact}) = -2\sin\beta\int_{0}^{\psi_\infty} \bar{w}\,d\psi \qquad (22)$$

$$M_0(\text{calc}) = \tfrac{1}{2}\int_{-\bar{X}}^{\bar{X}} p\bar{x}\,d\bar{x}$$

$$M_0(\text{exact}) = \bar{x}_s F(\text{exact}) \qquad (23)$$

From a moment balance about $\bar{x}_s$, the location of the resultant force, it can be seen by inspection that $\bar{x}_s$ is also the distance from the jet centerline to the stagnation streamline measured at the jet exit and along the direction parallel to the ground plane (Fig. 1).

It is demonstrated (Table 3) that the computed force and moment are in error by at most 3% and 2%, respectively,

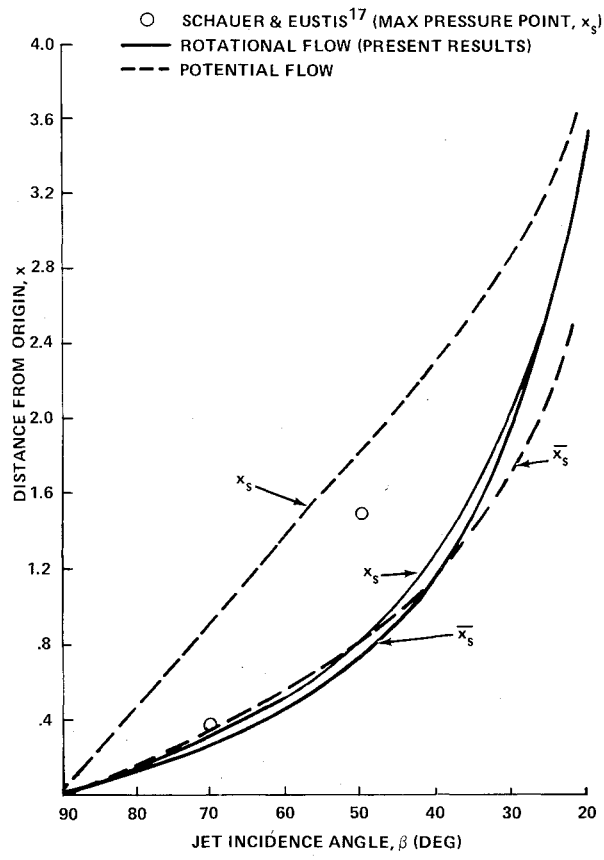

Fig. 11 Ground plane location of resultant force and stagnation point for rotational, irrotational jets ($\bar{x}_s$, resultant force; x_s, stagnation point).

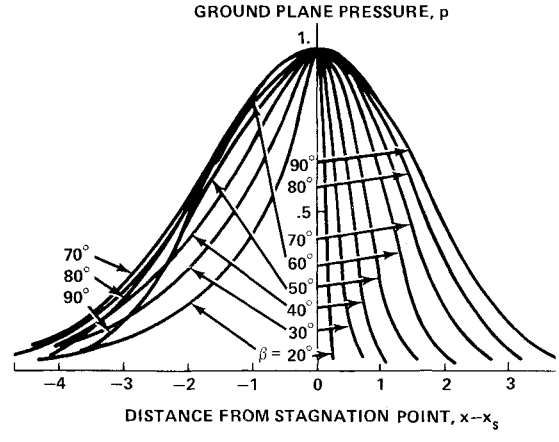

Fig. 12 Potential flow ground plane pressure distribution for two-dimensional oblique jet impingement.

indicating that the oblique impingement cases are sufficiently converged.

The computations require about 10^{-3} s/iteration/(number of points) and have been performed using an HP 3000 Series II computing system (a factor of about 20 relates this time to IBM 370-168 time). Few experiments have been done to optimize the relaxation parameter; the cases of Table 2, except for the developing profiles, used $r = 1$. The cases listed in Table 2 are those used to demonstrate convergence properties and quite satisfactory solutions can be obtained for many of the cases with considerably less stringent conditions. Finally, although the cases presented here include impingement angles down to 30 deg, the limitation is on physical rather than numerical grounds; converged computations have been established for β as low as 10 deg.

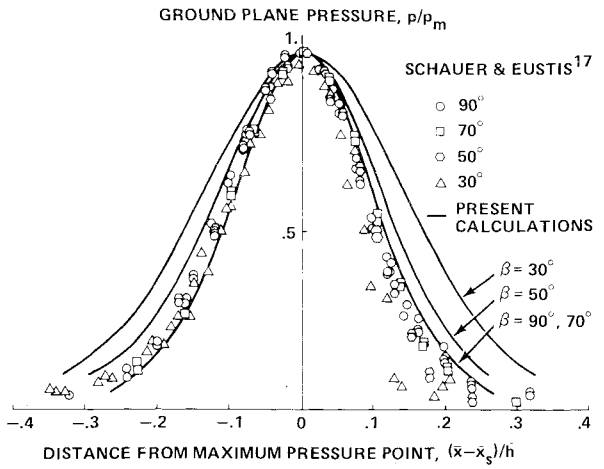

Fig. 13 Comparison of computed and observed ground plane pressure distributions for two-dimensional impingement.

Results and Discussion

The computations described herein are for idealized inviscid rotational jets located far from the impingement plane with lengths scaled by the jet half-width and pressures by the maximum jet total pressure. Real jets, however, encounter a free-mixing zone prior to entry into the impingement region and data are usually presented with length scales given by either the jet height above ground or the half-width of the undisturbed jet at the ground plane. If a matching point between the computed solution and point of free jet entry to the impingement zone is established then the free jet length scales can be related to the computational length scale by well-known free-jet spreading rate parameters.[9,12,13] In presenting the computation/data comparisons, it is convenient to use the rotational jet length scale so that dimensionless jet heights, h, are always referred to this quantity. The ground pressure data are normalized by the peak ground plane pressure, p_m, to eliminate total pressure loss considerations. All pressures are measured relative to ambient.

For normal axisymmetric impingement, Giralt et al.[12] use the criterion that the impingement region commences when the centerline velocity is 98% of that in the undisturbed free jet at the identical distance from the nozzle exit. According to the present computations, the location of this point is at $z \simeq 2.1$, which is in close agreement with the value $z \simeq 2.2$ observed by Giralt et al. Comparison of the calculated ground plane pressure distribution with data[9,12] (Fig. 4) shows excellent agreement over the entire range of the distribution. This is a considerable improvement upon the inviscid solution of Scholtz and Trass[13] which breaks down at large distances from the centerline. The agreement between the current computations and those of Scholtz and Trass for velocity decay along the centerline is demonstrated in Fig. 5; the discrepancy with respect to the data[13,14] is attributed to mixing phenomena within the impingement zone.[12]

Comparison of the results for the normal impingement of fully developed two-dimensional jets proceeds in a similar manner. Numerical computations yield the 98% criterion at $z \simeq 3.46$ which, in conjunction with accepted spreading rates,[11] provides the relationship $h \simeq 12.2$, where, again h is the dimensionless distance from the jet exit to the ground plane. The calculations (Fig. 6) indicate that for this case, too, there is excellent agreement with observations.

If the jet exit plane is in proximity to the ground plane (but outside the impingement zone), then a core region is present and a developing velocity profile exists at the beginning of the impingement zone. The computations of ground plane pressure under such conditions are shown in Fig. 7 and are seen to fall between the potential flow solution[18] and the fully developed rotational flow solution. A comparison with the data of Gardon and Akfirat,[15] assuming that the half-width is half the jet width (i.e., core flow is present), shows that the measured ground plane pressures are between the computed developing flow cases $\sigma = 0.1$ and $\sigma = 0.25$. Qualitatively similar results are found in the axisymmetric case when data[12,19] are compared with the potential flow solution of Strand.[20] From Bower et al.'s[4] data, obtained with a curved confining plate around the two-dimensional jet exit, the half-width at the impingement zone is estimated to be 1.16 jet widths, in reasonable agreement with the assumption of a developing flow. The ground plane pressure data differ little from the present calculations, but a solution to the full Navier-Stokes equations by Bower et al.[4] shows significant error (Fig. 7). The confining plate, which can be the source of a discrepancy vis-a-vis the inviscid calculations, is not expected to influence the results near the centerline.[21] Figure 8 demonstrates that the centerline velocity decay is closely represented by the developing flow case $\sigma \simeq 0.5$, while the Navier-Stokes representation[4] still produces poor results. It is noted, however, that close-ground effect Navier-Stokes calculations ($h \simeq 4$) have proven more successful.[3]

Table 4 Dimensionless jet impingement zone height $\bar{z}$ and free jet exit plane height $\bar{h}$ measured from ground plane along jet centerline as a function of impingement angle

β, deg	$\bar{z}$	$\bar{h}$	$\bar{z}/\bar{h}$
90	3.46	12.2	0.28
80	3.51	12.2	0.28
70	3.57	12.3	0.29
60	3.83	12.5	0.31
50	4.13	12.8	0.32
40	4.84	13.5	0.36
30	5.78	14.5	0.40

Computation of two-dimensional, oblique impingement produces the flow configurations depicted in Fig. 9. As the jet inclination angle, β, decreases from 90 deg, the stagnation streamline shifts, according to Eq. (14) in order to maintain the momentum balance. This shift reduces the total pressure of the stagnation streamline (Fig. 10), although the pressure distributions still appear to be symmetric about the peaks. The calculations show (Fig. 9) that for fully developed jets, the stagnation streamlines approach the ground plane with virtually no deflection. A Taylor series expansion of the stream function about the stagnation point shows that the stagnation line incidence angle, β_s, is related to the velocity gradient at the stagnation point, $(\partial u/\partial x)_s$, and the jet vorticity distribution by

$$\tan\beta_s = -\frac{2(\partial u/\partial x)_s}{\omega(x_s)} \tag{24}$$

where $\omega(x_s)$ is the vorticity on the stagnation streamline. This relationship, which is well satisfied in the numerical calculations, serves to verify the computational results and indicates that for a uniform (potential) jet the stagnation streamline is perpendicular to the ground plane. It is instructive to compare further the rotational and potential jet cases. The location $\bar{x}_s$ of the resultant force is almost identical for the two cases over the range 30 deg $\leq \beta \leq$ 90 deg, but the deflection of the uniform jet stagnation streamline causes a significant displacement of the maximum pressure point,[22] x_s, whereas $\bar{x}_s$ and x_s are virtually coincident for the fully developed jet (Fig. 11). The separation, $x_s - \bar{x}_s$, implies a ground plane pressure distribution[18] that is asymmetric about the stagnation point (Fig. 12) in contrast to the result for the fully developed jet.

The data of Schauer and Eustis[17] are compared with the present computations for the fully developed jet by again relating jet heights and half-widths (Table 4). The observed maximum pressure point location (Fig. 11) is in agreement

with the computations at $\beta = 70$ deg, but deviates with reduced impingement angles. Included in the calculated results is a case with $\beta = 20$ deg in order to illustrate that the magnitude of the observed trends are recovered by the computations.

The ground plane pressure distribution data exhibit symmetry about the maximum pressure point as suggested earlier and are well represented by the calculations for 60 deg $\lesssim \beta \lesssim 90$ deg (Fig. 13). This is consistent with the range over which agreement is obtained for the location of the maximum pressure point. Quantitative disagreement between the computations and data at more shallow incidence angles is not unexpected. The calculated height of the impingement zone is 40% of the jet height at $\beta = 30$ deg (Table 4) which, along with order-of-magnitude arguments that can be invoked,[9,23] illustrates the increasing influence of the turbulent stress gradient terms and consequent breakdown of the inviscid rotational flow model at shallow impingement angles.

Conclusions

Numerical computations for a variety of rotational jet impingement problems are given here. From the results and discussion, it may be concluded that:

1) The inviscid rotational flow formulation provides an excellent description of the ground plane pressure distribution for normally impinging, fully developed axisymmetric and two-dimensional jets.

2) Ground plane pressure distributions and centerline velocity decays for normally impinging developing two-dimensional jets may also be represented by this technique and show improvement with respect to existing Navier-Stokes-type computations.

3) The structure of obliquely impinging fully developed two-dimensional jets is such that the stagnation streamline exhibits little deflection and the ground plane pressure distributions are symmetric about the stagnation point.

4) Quantitative agreement with observations is obtained for maximum pressure point location and ground plane pressure distribution for oblique jet impingement angles $\beta \gtrsim 60$ deg.

5) The extent of the impingement zone increases as the jet inclination angle drops (e.g., at $\beta = 30$ deg, it is 40% of the jet height) providing one indication that turbulent stress gradient terms become increasingly relevant in the impingement zone for $\beta \lesssim 60$ deg.

Acknowledgment

The author is indebted to R. Melnik and S. Rudman for suggesting this problem. This investigation was partially supported by the Office of Naval Research, Contract No. N00014-77-C-0524.

References

[1] Wolfshtein, M., "Some Solutions of the Plane Turbulent Impinging Jet," *Journal of Basic Engineering Transactions of ASME*, Vol. 92D, Dec. 1970, pp. 915-922.

[2] Bower, W. W. and Kotansky, D. R., "A Navier-Stokes Analysis of the Two-Dimensional Ground Effects Problem," AIAA Paper 76-621, Palo Alto, Calif., July 1976.

[3] Kotansky, D. R. and Bower, W. W., "A Basic Study of the VTOL Ground Effect Problem for Planar Flow," *Journal of Aircraft*, Vol. 15, April 1978, pp. 214-221.

[4] Bower, W. W., Kotansky, D. R., and Hoffman, G. H., "Computations and Measurements of Two-Dimensional Turbulent Jet Impingement Flowfields," *Symposium on Turbulent Shear Flows*, Vol. 1, University Park, Pa., April 1977.

[5] Siclari, M. J., Migdal, D., and Palcza, J. L., "The Development of Theoretical Models for Jet-Induced Effects on V/STOL Aircraft," *Journal of Aircraft*, Vol. 13, Dec. 1976, pp. 938-944.

[6] Siclari, M. J., Hill, Jr., W. G., and Jenkins, R. C., "Investigation of Stagnation Line and Upwash Formation," AIAA Paper 77-615, Palo Alto, Calif., June 1977.

[7] Siclari, M. J., Aidala, P., Wohllebe, F., and Palcza, J. L., "Development of Prediction Techniques for Multi-Jet Thermal Ground Flow Field and Fountain Formation," AIAA Paper 77-616, Palo Alto, Calif., June 1977.

[8] Sparrow, E. M. and Lee, L., "Analysis of Flow Field and Impingement Heat/Mass Transfer Due to a Nonuniform Slot Jet," *Journal of Heat Transfer Transaction of ASME*, Vol. 97C, May 1975, pp. 191-197.

[9] Bradbury, L.J.S., "The Impact of an Axisymmetric Jet onto a Normal Ground," *Aeronautical Quarterly*, Vol. 23, May 1972, pp. 141-147.

[10] Parameswaren, V. and Alpay, S. A., "Normal Impingement of Jets," *Journal of Aircraft*, Vol. 13, March 1974, pp. 189-191.

[11] Schlichting, H., *Boundary Layer Theory*, 4th ed., McGraw-Hill Book Co., Inc., New York, 1960, Chap. XXIII.

[12] Giralt, F., Chia, C. J., and Trass, O., "Characterization of the Impingement Region in an Axisymmetric Turbulent Jet," *Industrial and Engineering Chemistry, Fundamentals*, Vol. 16, Jan. 1977, pp. 21-28.

[13] Scholtz, M. T. and Trass, O., "Mass Transfer in a Nonuniform Impinging Jet Part I. Stagnation Flow-Velocity and Pressure Distribution," *AIChE Journal*, Vol. 16, Jan. 1970, pp. 82-90.

[14] Tani, I. and Komatsu, Y., "Impingement of a Round Jet on a Flat Plate," *Eleventh International Conference of Applied Mechanics*, Munich, 1964, Springer-Verlag, Berlin, 1966, pp. 672-676.

[15] Gardon, R. and Akfirat, J. C., "The Role of Turbulence in Determining the Heat-Transfer Characteristics of Impinging Jets," *International Journal of Heat and Mass Transfer*, Vol. 8, Oct. 1965, pp. 1261-1272.

[16] Cartwright, W. G. and Russell, P. J., "Characteristics of a Turbulent Slot Jet Impinging on a Plane Surface," Paper No. 32, Thermodynamics and Fluid Mechanics Convention, Inst. of Mech. Engineers, Bristol, England, March 1968.

[17] Schauer, J. J. and Eustis, R. H., "The Flow Development and Heat Transfer Characteristics of Plane Turbulent Impinging Jets," Dept. of Mechanical Engineering, Stanford University, TR 3, Sept. 1963.

[18] Milne-Thomson, L. M., *Theoretical Hydrodynamics*, 4th ed., Chap. XI, The Macmillan Co., New York, 1960.

[19] Hill, W.G. Jr., and Jenkins, R.C., "Experimental Investigation of Multiple Jet Impingement Flows Applicable to VTOL Aircraft in Ground Effect," Grumman Research Dept., RM-605, 1975.

[20] Strand, T., "On the Theory of Normal Ground Impingement of Axi-Symmetric Jets in Inviscid Incompressible Flow," AIAA Paper 64-424, 1964.

[21] Saad, N. R., Douglas, W.J.M., and Mujumdar, A. S., "Prediction of Heat-Transfer under an Axisymmetric Laminar Impinging Jet," *Industry and Engineering Chemistry, Fundamentals*, Vol. 16, Jan. 1977, pp. 148-154.

[22] Slezkin, N. A., "On Impact of a Plane Gas Stream Upon an Infinite Wall," *Prikladnaia Matematika I Mekhanika*, Vol. 16, No. 2, 1952, pp. 227-230.

[23] Foss, J. F. and Kleiss, S. J., "The Oblique Impingement of an Axisymmetric Jet," *Proceedings of Fourth Canadian Congress of Applied Mechanics*, Montreal, May 28-June 1, 1973.